Received: 18 December 2019 | Revised: 7 March 2020 | Accepted: 16 March 2020

DOI: 10.1002/aoc.5693

FULL PAPER

Applied Organometallic Chemistry WILEY

Synthesis and characterization of some binuclear metal complexes with a pentadentate azodye ligand: An experimental and theoretical study

Ashish Kumar Sarangi[1] | **Bipin Bihari Mahapatra**[2] | **Ranjan Kumar Mohapatra**[3] | **Sisir Kumar Sethy**[2] | **Debadutta Das**[4] | **Lucia Pintilie**[5] | **Md. Kudrat-E-Zahan**[6] | **Mohammad Azam**[7] | **Hemanta Meher**[8]

[1]Department of Chemistry, School of Applied Sciences, Centurion University of Technology and Management, Odisha, India

[2]P.G. Department of Chemistry, G.M. University, Sambalpur, Odisha, India

[3]Department of Chemistry, Government College of Engineering, Keonjhar, Odisha, India

[4]Department of Chemistry, Sukanti Degree College, Subarnapur, Odisha, India

[5]Department of Synthesis of Bioactive Substances and Pharmaceutical Technologies, National Institute for Chemical & Pharmaceutical Research and Development, Bucharest, Romania

[6]Department of Chemistry, Rajshahi University, Rajshahi, Bangladesh

[7]Department of Chemistry, College of Science, King Saud University, Riyadh, Saudi Arabia

[8]School of Chemistry, Sambalpur University, Burla, Odisha, India

Correspondence
Dr. Ashish Kumar Sarangi, Department of Chemistry, School of Applied Sciences, Centurion University of Technology and Management, Odisha, India.
Email: ashishsbp_2008@yahoo.com

Dr. Ranjan Kumar Mohapatra, P.G. Department of Chemistry, G.M. University, Sambalpur, Odisha, India.
Email: ranjank_mohapatra@yahoo.com

Dr. Bipin Bihari Mahapatra, Department of Chemistry, Government College of Engineering, Keonjhar, Odisha, India.
Email: mahapatra.bipin@yahoo.com

A novel series of binuclear complexes with Mn(II), Co(II), Ni(II), Cu(II), Zn(II), and Cd(II) ions derived from a pentadentate azo dye ligand (H_3L) was synthesized and structurally investigated by various physicochemical analyses, namely, scanning electron microscopy, transmission electron microscopy, NMR, UV–visible spectroscopy, and Electron-Spin Resonance (ESR) studies. The infrared spectral data revealed characteristic bands due to ν(N=N) and ν(C=O) at 1606 and 1631 cm^{-1} in the free ligand. However, their positions shifted and appeared at ~1564 and ~1592 cm^{-1} on coordination, suggesting the involvement of carbonyl oxygen and azo nitrogen in complex formation. The spectral data suggested octahedral geometry for the complexes. The kinetic parameters such as order and activation energy were determined from the thermal decomposition values. X-ray powder diffraction analysis showed the orthorhombic nature of the cadmium complex. Furthermore, Density functional theory (DFT) calculations were also recorded to describe the insight bonding. The synthesized compounds were tested for *in vitro* antibacterial activity against *K. aerogenes*, *S. aureus*, *B. acidoterrestris*, *E. coli*, and *V. cholerae* strains by the cup-plate method. In addition, the interactions that occurred in the protein–ligand complexes have been predicted by docking analysis.

KEYWORDS

antibacterial studies, DFT calculations, molecular docking studies, pentadentate azodye ligand, SEM study

1 | INTRODUCTION

The excessive use of antimicrobials has been a major factor in the rise of drug-resistant microbes, which remain a leading cause of death worldwide. Because of a lack of effective treatments, microbial infections cause serious problems to humankind. Therefore, to overcome the growing resistance of antimicrobial agents, researchers are developing new classes of antimicrobial drugs with adequate mechanisms. In recent years, transition metal complexes,[1–5] which have attracted substantial interest in bioinorganic chemistry as metal-based drugs, have been found to be good candidates for their efficacy.

Azo dyes are organic compounds bearing the coloured azo function (–N=N–) bound to aryl groups. The presence of the active azo group makes them a class of ligands with the ability to bind a number of metal ions in different oxidation states. These are irrefutably the most preferred ligands after Schiff bases for the synthesis of coordination compounds due to their remarkable chelating ability. The chemistry of azo dye compounds and their metal complexes is truly exciting owing to their plethora of applications in diverse and promising areas. Most importantly, the therapeutic uses of such compounds are undoubtedly beneficial to humankind. Compounds containing potential azo groups possess strong antifungal,[6] antimicrobial,[7] and anticancer[8–10] properties. To enhance the pharmacological properties of these compounds they can be complexed with various transitional and nontransitional metal ions.[11]

Furthermore, azo dyes are one of the most commonly used chromophores in the dye industry. Because of their pigment properties, they are also used in photoelectronics[12] and leather technology. Biological reactions such as protein synthesis, inhibition of DNA and RNA, and the nitrogen fixation process are carried out using azo dye compounds. We have already synthesized a number of azo dye ligands with O, N, and S donor atoms and their metal complexes.[13–16] This study describes the synthesis of one novel pentadentate azodye ligand (Scheme 1) and its binuclear transition metal complexes. The reported compounds were screened against some selected microbes to establish their *in vitro* antimicrobial activity. In addition, DFT, quantitative structure–activity relationship (QSAR) and molecular docking studies were carried out.

2 | EXPERIMENTAL

2.1 | Materials

For the synthesis, we used chemicals, reagents, solvents, and metal salts of analytical grade (E. Merck) as received.

2.2 | Synthesis of the ligand

Anthranilic acid (0.01 mol, 0.9 g) was reacted with a mixture of sodium nitrate and HCl. The resulting solution was then gradually added to an alkaline solution of 2,4-dihydroxyacetophenone (0.01 mol, 1.1 g) at freezing temperature. The azodye (2′,4′-dihydroxy-5′-acylphenylazo)-2-carboxybenzene, H_3L) was separated out and purified. The schematic representation for the synthesis of the azo dye ligand H_3L is shown in Scheme 1.

H_3L: molecular formula $C_{15}H_{12}N_2O_5$ (300.27), m.p. >250°C. Anal. calcd (%): C 60, H 4.03, N 9.3; found (%): C 59.8, H 3.9, N, 9.1. IR (KBr pellet cm^{-1}): 1495 (C–O), 1606 ν(N=N), 1630 ν(C=O). ^{13}C NMR δ: 27.0 (C1), 104.0, 108.0, 114.0, 129.0, 132.0, 135.0 (Ar–C), 163.0 (C4), 165.0 (C6), 204.0 (C2).

2.3 | Synthesis of the metal complexes

The ligand solution in ethanol was reacted with metal chloride in 1:2 molar ratio The resulting solution was refluxed for 1 hr at 50–60°C followed by the addition of conc. NH_4OH with constant stirring until the pH was maintained at ~7. The precipitate was separated off,

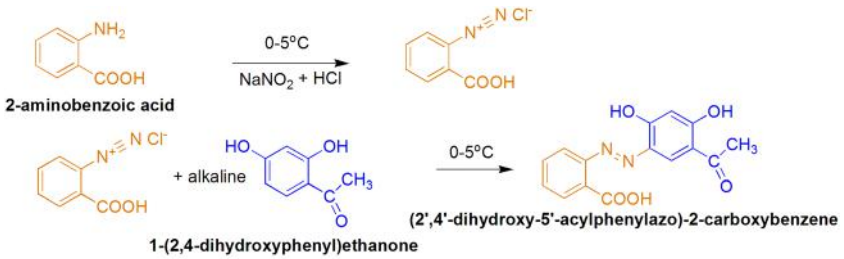

Scheme 1: Synthesis of azo dye ligand, H_3L

SCHEME 1 Synthesis of azo dye ligand H_3L

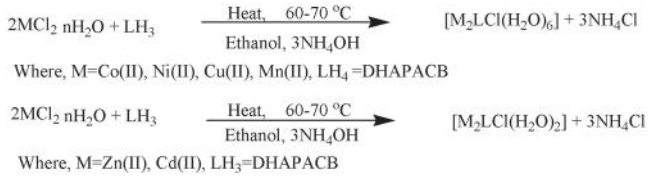

SCHEME 2 Synthesis of azo dye metal complexes

washed with deionized water, and finally dried in vacuum (Scheme 2).

$[Co_2(L)Cl(H_2O)_2]$ (brown): molecular formula $C_{15}H_{21}ClCo_2N_2O_{11}$ (558.6), m.p. >250°C. Anal. calcd (%): C 32.2, H 3.7, N 5.0, Cl 6.3, Co 21.1; found (%): C 31.9, H 3.3, N 5.5, Cl 6.0, Co 21.5. IR (KBr pellet cm^{-1}): 1430 (C–O), 1486 ν(N=N), 1598 ν(C=O), 571 (M–O), 495 (M–N).

$[Ni_2(L)Cl(H_2O)_6]$ (faint green): molecular formula $C_{15}H_{21}ClNi_2N_2O_{11}$ (558.1), m.p. >250°C. Anal. calcd (%): C 32.2, H 3.7, N 5.0, Cl 6.3, Ni 21.0; found (%): C 31.8, H 3.5, N 5.5, Cl 6.5, Ni 21.3. IR (KBr pellet cm^{-1}): 1474 (C–O), 1564 ν(N=N), 1592 ν(C=O), 572 (M–O), 461 (M–N).

$[Cu_2(L)Cl(H_2O)_6]$ (deep green): molecular formula $C_{15}H_{21}ClCu_2N_2O_{11}$ (567.8), m.p. >250°C. Anal. calcd (%): C 31.7, H 3.7, N 4.9, Cl 6.2, Cu 22.3; found (%): C 31.4, H 3.3, N 4.8, Cl 6.5, Cu 22.7. IR (KBr pellet cm^{-1}): 1439 ν(C-O), 1503 ν(N=N), 1594 ν(C=O), 581 (M–O), 480 (M–N).

$[Mn_2(L)Cl(H_2O)_6]$ (purple): molecular formula $C_{15}H_{21}ClMn_2N_2O_{11}$ (550.6), m.p. >250°C. Anal. calcd (%): C 32.7, H 3.8, N 5.0, Cl 6.4, Mn 19.9; found (%): C 32.2, H 4.2, N 5.4, Cl 6.5, Mn 19.5. IR (KBr pellet cm^{-1}): 1415 (C–O), 1480 ν(N=N), 1585 ν(C=O), 572 ν(M–O), 490 (M–N).

$[Zn_2(L)Cl(H_2O)_2]$ (brown): molecular formula $C_{15}H_{13}ClZn_2N_2O_7$ (499.5), m.p. >250°C. Anal. calcd (%): C 36.0, H 2.6, N 5.6, Cl 7.1, Zn 26.1; found (%): C 35.6, H 2.1, N 5.2, Cl 7.4, Zn 26.3. IR (KBr pellet cm^{-1}): 1430 (C–O), 1486 ν(N=N), 1584 ν(C=O), 528 ν(M–O), 475 (M–N).

$[Cd_2(L)Cl(H_2O)_2]$ (grey): molecular formula $C_{15}H_{13}ClCd_2N_2O_7$ (593.5), m.p. >250°C. Anal. calcd (%): C 30.3, H 2.2, N 4.7, Cl 5.9, Cd 37.8; found (%): C 30.1, H 2.4, N 4.9, Cl 6.0, Cd 37.5. IR (KBr pellet cm^{-1}): 1433 (C–O), 1497 ν(N=N), 1600 ν(C=O), 526 ν(M–O), 482 (M–N).

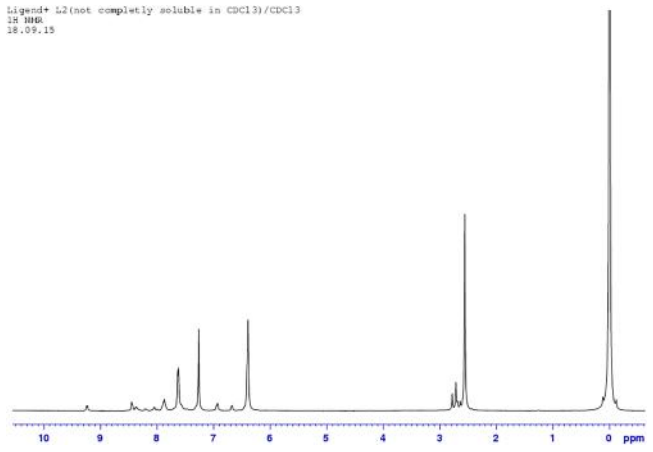

FIGURE 1 ^{1}H NMR spectrum of ligand H_3L

2.4 | Physical measurements

The C, H and N were determined on a Perkin-Elmer 2400 Elemental analyzer. The electronic spectra of the compounds in dimethyl formamide (DMF) were recorded on a Hilger-Watt uvispeck spectrophotometer. The Gouy technique was used to study the magnetic effects at room temperature. The ^{1}H and ^{13}C NMR spectra were obtained

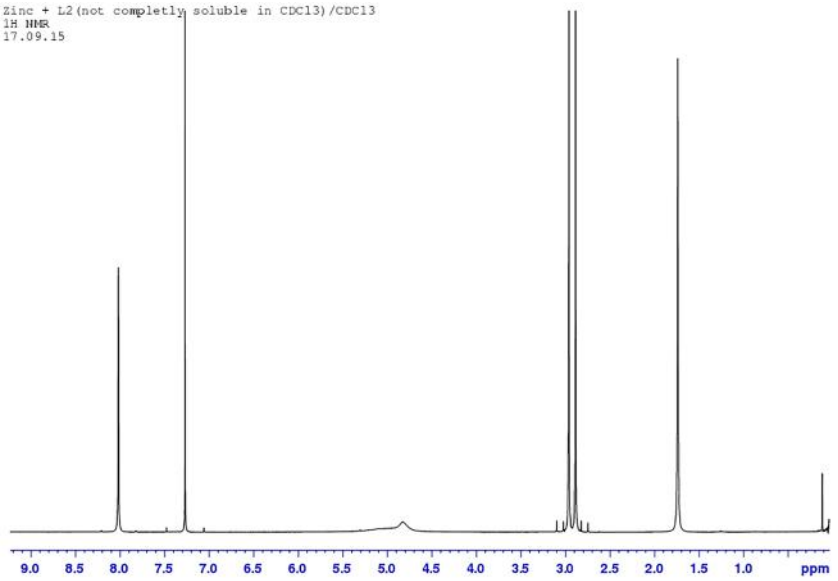

FIGURE 2 ^{1}H NMR spectrum of Zn(II) complex

by a Jeol GSX 400 with $CDCl_3$ as solvent. The ESR spectrum of the Cu(II) complex was recorded on an E_4 spectrometer. The ESI-MS analysis was done by micrOTOF-Q ‖ 10337. The powder X-ray diffraction (XRD) of the cadmium complex was performed on a Phillips PW1130/00 diffractometer. The scanning electron microscopy (SEM) image was obtained by using a Jeol model JSM-5410. The Energy-dispersive X-ray spectroscopy (EDX) was carried out using an EDX (TESCAN) X-max version 4.1.17.D/Mi 152. The thermal analyses were recorded on a NETZSCH STA 409 C/CD in a nitrogen environment at a heating rate of 10°C per minute.

2.5 | Computational (DFT) studies

All the synthesized compounds were first optimized and the optimized geometry was studied with the help of Gauss View 5.0.8.[17] The DFT evaluations were made using the GAUSSIAN 03 rev. A.01 suit programme[18–24] by applying the DFT/B3LYP level of theory with the LANL2DZ basic set for metal atoms and the 6–31G(d, p) basic set for carbon, hydrogen, nitrogen, and oxygen atoms.

2.6 | In vitro antibacterial study

The *in vitro* antibacterial activity of these azo dye compounds was investigated against *K. aerogenes*, *S. aureus*, *B. acidoterrestris*, *E. coli*, and *V. cholerae* as per the cup-plate method.[25] The solutions were prepared in dimethyl sulfoxide (DMSO) at 500 μg/ml. Tetracycline was used as the standard drug for reference. The study was carried out according to the previously reported

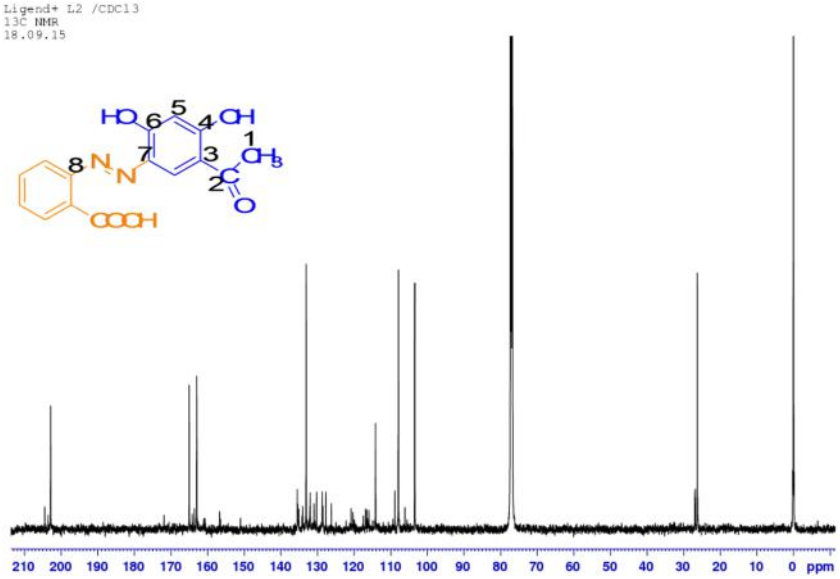

FIGURE 3 ^{13}C NMR spectrum of H_3L

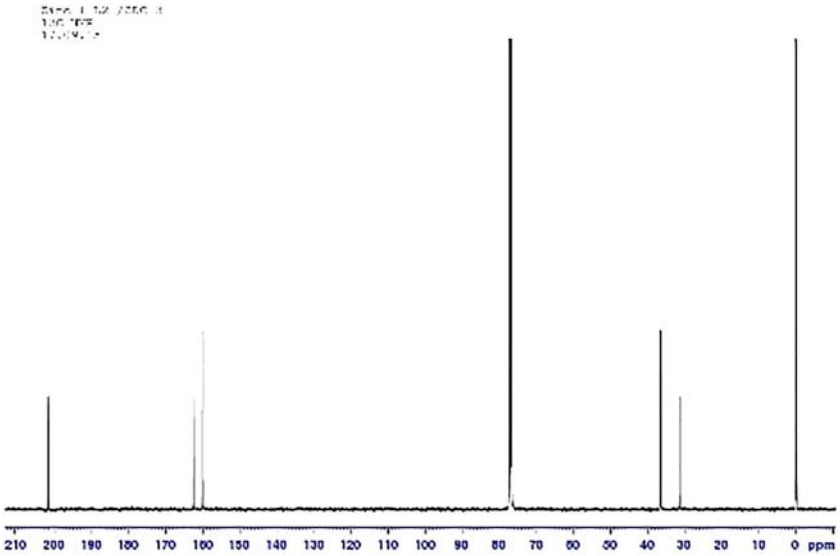

FIGURE 4 ^{13}C NMR spectrum of Zn(II) complex

method.[26] Finally, the zone of inhibition was measured using the Vernier scale.

3 | RESULTS AND DISCUSSION

The chemical compositions of the metal complexes $[M_2LCl(H_2O)_6]$ and $[M'_2LCl(H_2O)_2]$ where M = Co(II), Ni(II), Cu(II), Mn(II) and M′ = Zn(II), Cd(II) were confirmed through elemental data. These complexes are amorphous and soluble in DMF and DMSO. The low conductance values (3.5–5.4 $\Omega^{-1}\cdot cm^2\cdot mol^{-1}$) in 10^{-3} M DMF solution indicates the nonelectrolytic nature of all the complexes.

3.1 | I R spectra

The sharp bands at 1606 and 1631 cm^{-1} were assigned to ν(N=N) and ν(C=O) for the azo dye ligand H_3L. However, these bands were shifted and appeared at ~1564 and ~1592 cm^{-1} in the metal complexes, indicating coordination through the carbonyl oxygen and azo nitrogen atoms.[27] A sharp band at 1495 cm^{-1} assigned to ν(C–O) in the free ligand was shifted to ~1474 cm^{-1} in the metal complexes, confirming coordination through phenolic oxygen atom. Furthermore, broad bands at

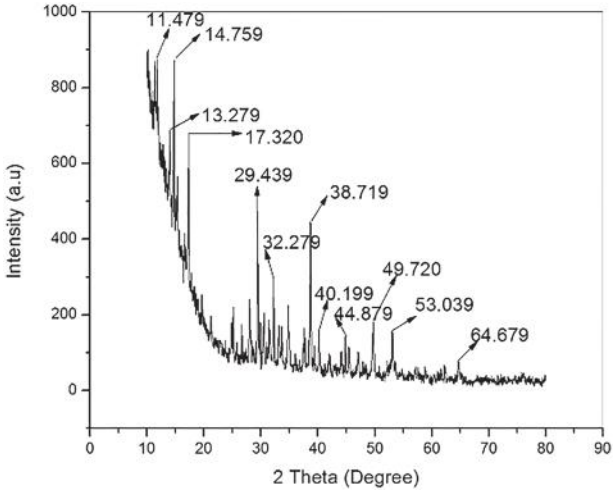

FIGURE 7 Powder XRD of $[Cd_2LCl(H_2O)_2]$

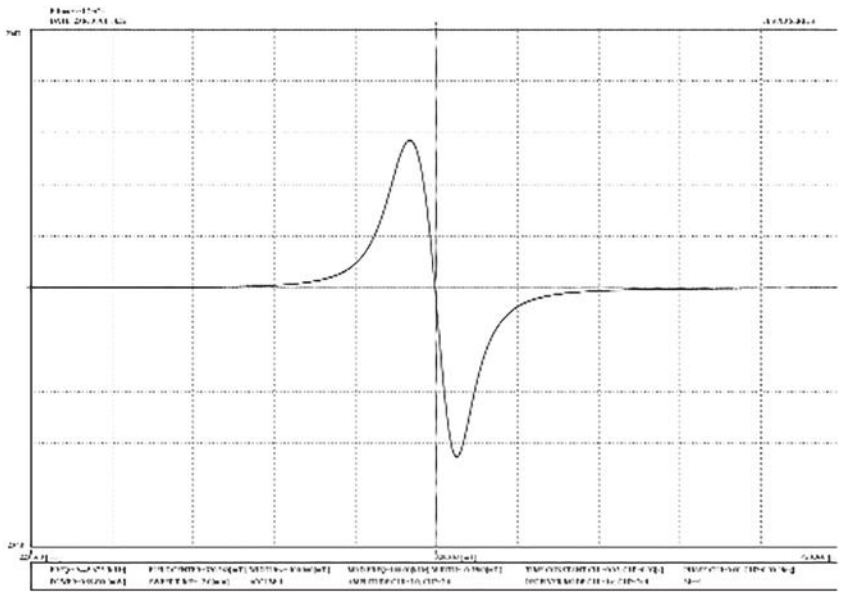

FIGURE 5 ESR spectrum of $[Cu_2LCl(H_2O)_6]$

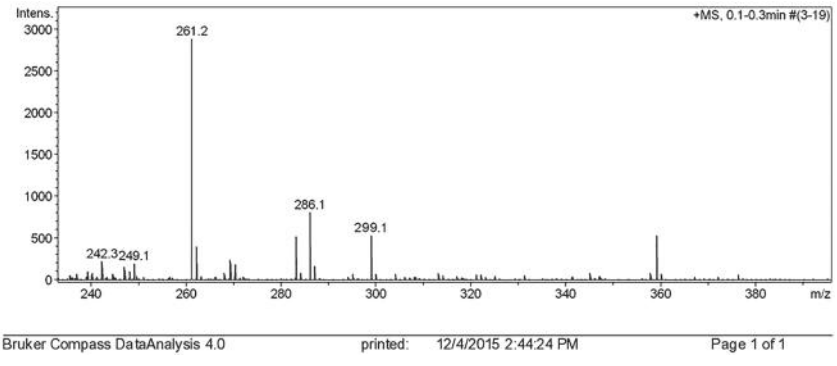

FIGURE 6 ESI-MS spectrum of H_3L

~3395 cm^{-1} followed by prominent peaks at ~856 and ~694 cm^{-1} were assigned to –OH stretching, wagging, and rocking vibrations, respectively,[28] indicating the existence of coordinated water. Additionally, the bands at ~572 and ~461 cm^{-1} ascribed to ν(M–O) and ν(M–N) vibrations further confirmed the involvement of metal ions in coordination.[29]

3.2 | Electronic spectra and magnetic measurements

Four bands seen in the cobalt complex at 8265, 16590, 20550 and 32205 cm^{-1} were assigned to $^4T_{1g}(F) \rightarrow {}^4T_{2g}(F)$ (ν_1), $\rightarrow {}^4A_{2g}(F)$ (ν_2), $\rightarrow {}^4T_{1g}(P)$ (ν_3), and Charge Transfer (CT) transitions, respectively.[30,31]

TABLE 1 X-ray diffraction data for the complex [Cd2LCl(H2O)2]

Observed 2θ	Calculated 2θ	d-spacing	h k l	Difference (2θ)
10.15	10.12	8.735	1 0 10	0.03
15.12	15.11	5.851	0 1 1	0.01
27.31	27.30	3.263	1 3 1	0.01
31.47	31.44	2.843	3 1 0	0.03
38.31	38.30	2.347	2 2 2	0.01
41.63	41.62	2.167	–1 1 3	0.01
44.03	44.01	2.056	0 6 1	0.02
49.47	49.45	1.841	2 6 1	0.02
54.47	54.43	1.684	–2 7–1	0.04
63.59	63.55	1.463	0 4 4	0.04

a = 10.614 Å, α = 90°, volume = 1044.45 $Å^3$, Bravais lattice = i.
b = 11.384 Å, β = 90°, density = 0.5 g/cm^3, figure of merit = 8.25.
c = 8.647 Å, γ = 90°, number of unit cells (n) = 1.5.
Crystal system = orthorhombic.

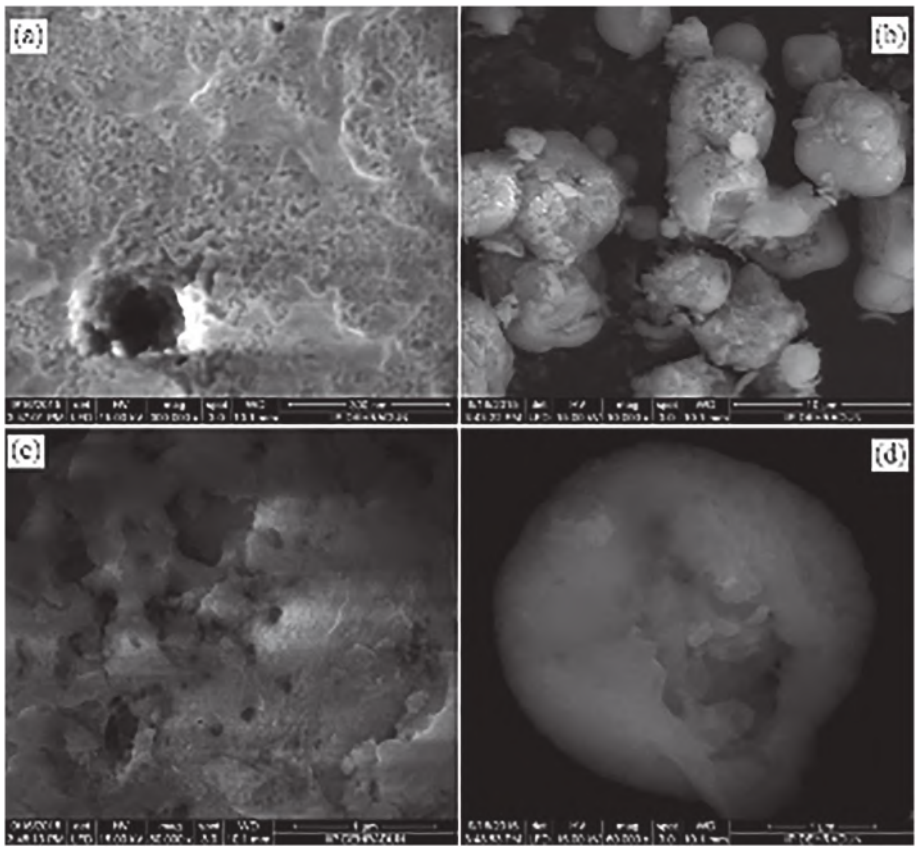

FIGURE 8 SEM micrograph of $[Cd_2LCl(H_2O)_6]$ complex

The ligand field parameters Dq = 832.5 cm^{-1}, B = 823 cm^{-1}, β_{35} = 0.847 cm^{-1}, ν_2/ν_1 = 2.007, and σ = 18.06% for the cobalt complex supported its octahedral configuration.[32,33] The nickel complex revealed four bands at 10235, 17520, 24850 and 32750 cm^{-1} consistent with $^3A_{2g}(F) \rightarrow {}^3T_{2g}(F)\,(\nu_1), \rightarrow {}^3T_{1g}(F)\,(\nu_2), \rightarrow {}^3T_{1g}(P)\,(\nu_3)$, and CT transitions, respectively, suggesting an octahedral geometry.[30] The ligand field parameters Dq = 728.5 cm^{-1}, B = 777.6 cm^{-1}, β_{35} = 0.747 cm^{-1}, ν_2/ν_1 = 1.711, and σ = 33.86% were determined. However, the copper complex exhibited one broad band at ~13355–14570 cm^{-1}, ascribed to the $^2Eg \rightarrow {}^2T_{2g}$ transition, suggesting an octahedral configuration.[34,35] The manganese complex showed four bands at 18870, 21075, 31690 and 36680 cm^{-1}, assigned to the $^6A_{1g} \rightarrow {}^4T_{1g}$ (^4G), $\rightarrow {}^4E_g$, $^4A_{1g}$ (^4G), $\rightarrow {}^4E_g$ (^4D) and $^4T_{1g}$ (^4P) transitions, respectively, supporting an octahedral geometry[36] (Supporting Information Table S1). The magnetic moment values of the Co(II), Ni(II), Cu(II), and Mn(II) complexes were found to be 5.1, 3.0, 1.8, and 5.9 B.M., respectively, which suggests an octahedral configuration around the metal ions[37,38] (Supporting Information Table S1).

3.3 | NMR studies

Proton resonance was observed at δ 6.4–7.9 ppm in the free ligand, corresponding to six phenyl protons.[39] One sharp peak corresponding to three methyl protons was observed at δ2.6 ppm (Figure 1). However, these values showed deshielding on coordination to Zn(II) ion. The resonance at 2.9–3.0 ppm in the zinc complex with integration correlating to four protons was ascribed to two water molecules[40] (Figure 2). The disappearance of signals due to phenolic and carboxylic protons confirmed their coordination through deprotonation.

The ^1H NMR data was further ascertained by ^{13}C NMR studies exhibiting a signal due to a $-CH_3$ group (C1) at 27 ppm in the azo dye ligand (Figure 3). A signal due to the >C=O group (C2) was observed at 204 ppm, whereas signals due to C–O groups were noticed at 163 (C4) and 165 (C6) ppm. The signals due to aromatic carbons appeared at 104.0–135.0 ppm. However, the position for signals due to phenolic and carbonyl carbon underwent deshielding, suggesting their involvement in coordination with the Zn(II) ion[41] (Figure 4).

3.4 | ESR studies

The ESR spectrum for the copper complex was measured at the X-band at room temperature with corresponding g_1, g_2, and g_3 values at 2.0219, 2.0798 and 2.2548, respectively.[42,43] However, the axial symmetry value G at 4.380 suggested that magnetically equivalent Cu(II) ions in the unit cell do

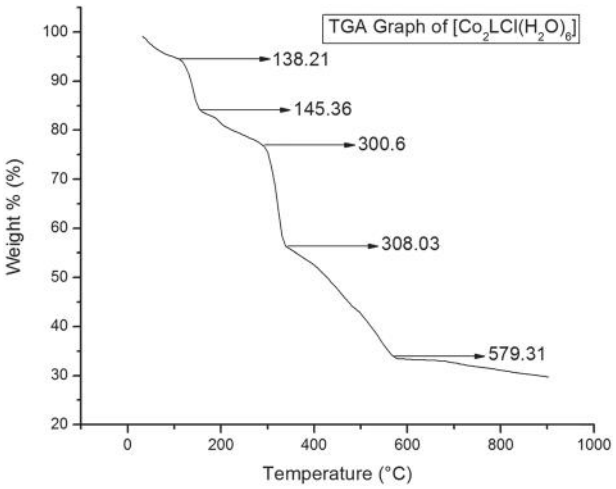

FIGURE 10 TGA graph of $[Co_2LCl(H_2O)_2]$

FIGURE 9 EDX microanalysis spectrum of $[Cd_2LCl(H_2O)_6]$

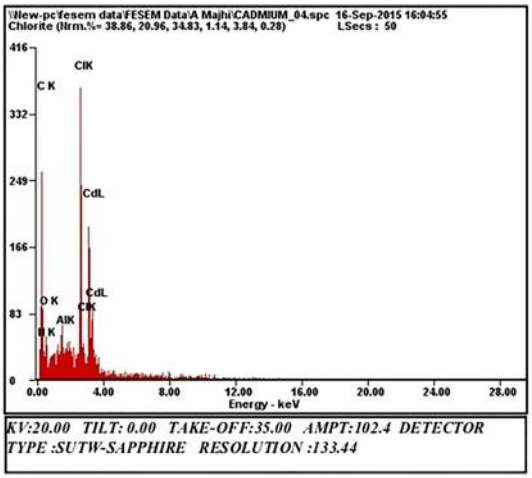

Element	Wt %	At %
C K	55.21	72.70
N K	10.67	12.05
O K	08.69	08.59
AlK	00.63	00.37
ClK	09.18	04.09
CdL	15.63	02.20

EDAX ZAF QUANTIFICATION STANDARDLESS SEC
TABLE : DEFAULT

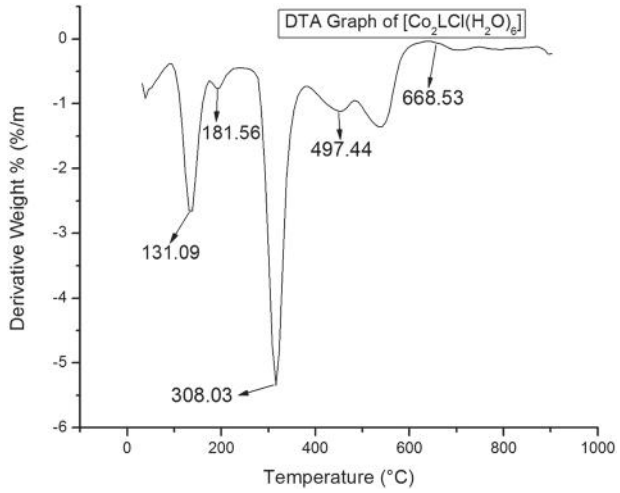

FIGURE 11 DTA graph of $[Co_2LCl(H_2O)_2]$

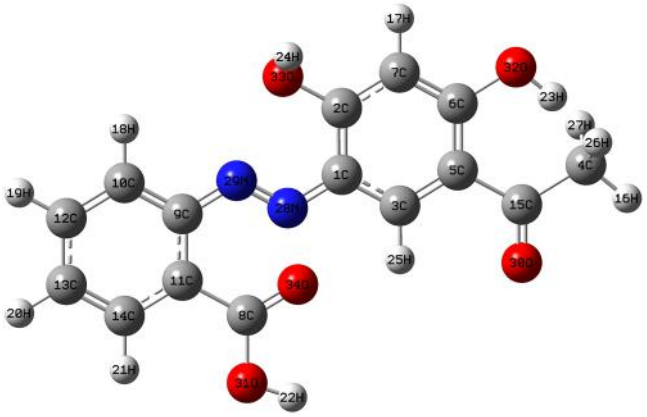

FIGURE 12 Optimized geometry of the ligand H_3L

not show any exchange interaction. The ground state information R (0.3308) can be obtained from the following equation, and is suggested to be predominant over $d_{x^2-y^2}$:

$$R = \frac{g_2 - g_1}{g_3 - g_2}$$

The spin-orbit coupling constant (ϰ) (−377.38 cm^{-1}) was calculated using the following relation:[14,43]

$$g_{av} = 2(1 - 2\varkappa/10Dq)$$

The reduced ϰ value (−377.3 cm^{-1}) obtained from the free ion value (−832 cm^{-1}) prominently exhibited the overlapping of metal ligand orbitals (Figure 5).

3.5 | Mass spectra

The ESI-MS spectrum of the ligand H_3L exhibited a peak with m/z 299.1, consistent with its molecular weight (Figure 6). The peak at m/z 286.1 may be due to the loss of methyl groups, whereas the peak at m/z 261.2 was assigned to the loss of the carbonyl group.

3.6 | Powder XRD studies

The powder XRD spectrum of the cadmium complex was recorded (Figure 7) and examined with the help of LSUCRPC software.[44] The value was ascertained by

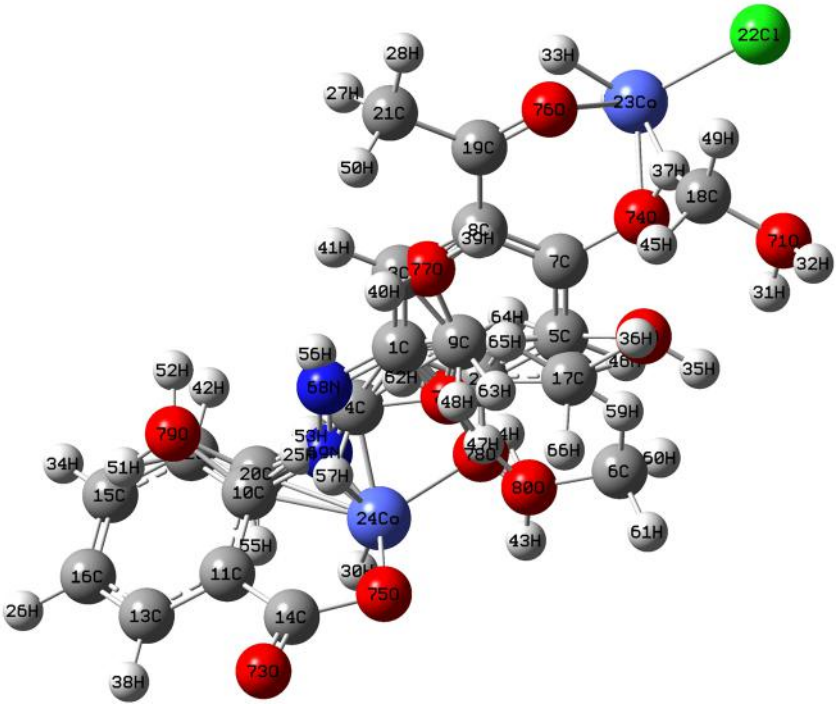

FIGURE 13 Optimized geometry of $[Co_2(L)Cl(H_2O)_6]$

comparing the experiential and calculated 2θ values (Table 1) and confirmed with a figure of merit 8.2.[45] The complex density (d) was ascertained by the floatation method individually in a saturated solution of NaCl, KBr, and benzene. The unit cell (n) was obtained from the following equation:

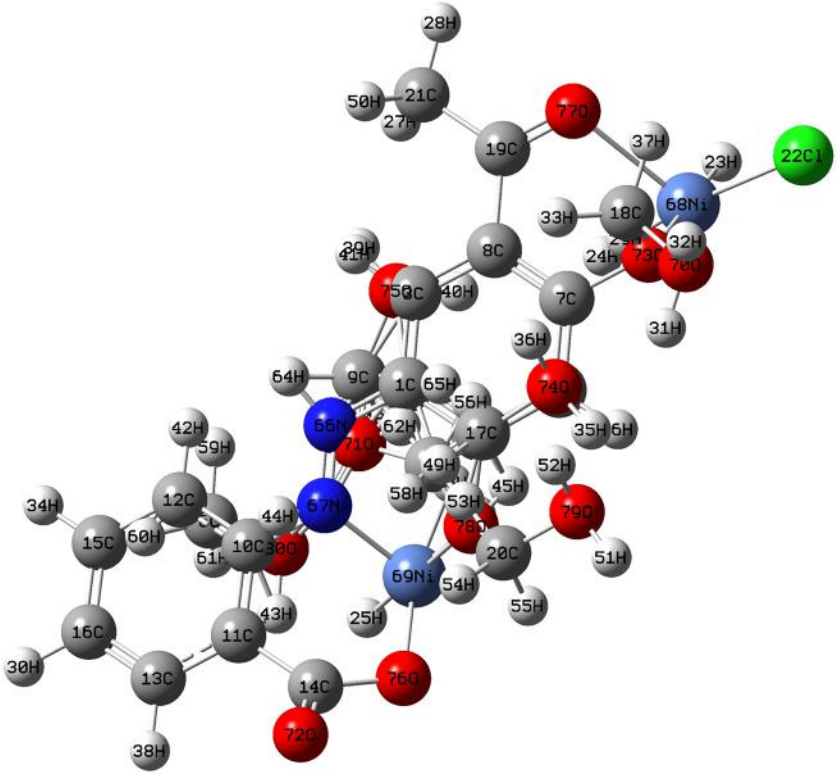

FIGURE 14 Optimized geometry of $[Ni_2(L)Cl(H_2O)_6]$

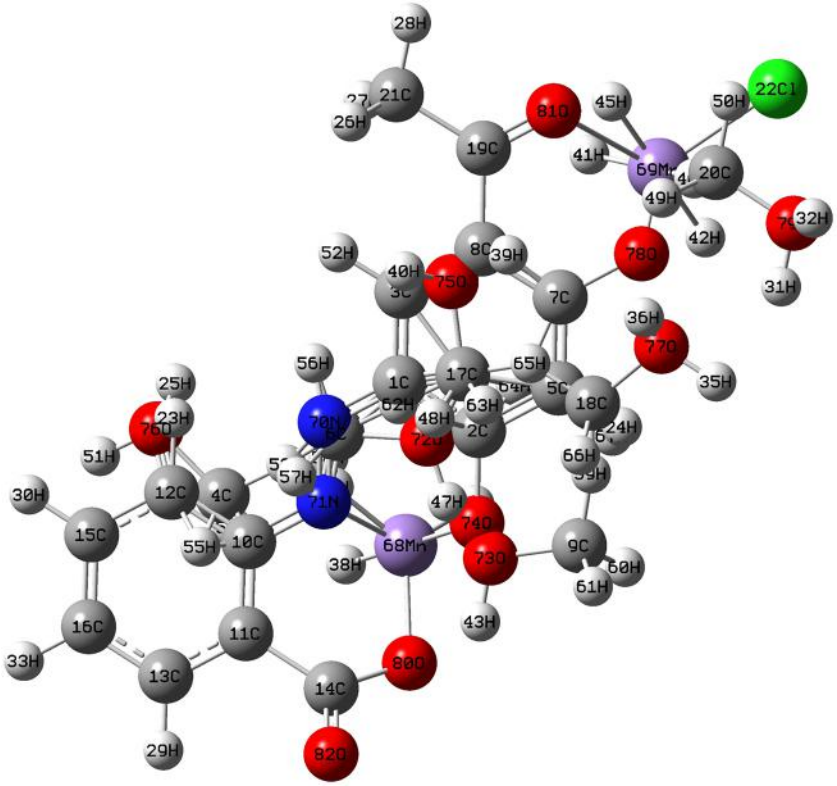

FIGURE 15 Optimized geometry of $[Mn_2(L)Cl(H_2O)_6]$

$$n = \frac{dNV}{M}$$

where d is density, N is Avogadro's number, V is volume, and M is the molecular weight of the complex. The calculated value of n at 1.5 suggests the orthorhombic crystalline structure of cadmium complex. The mean particle size of the cadmium complex at 8.1 nm, shown in the broadening of the peak in the diffraction pattern, was obtained from the Debye Scherer equation[46]:

$$D = K\lambda/\beta\cos\theta$$

where D is particle size, K is the dimensionless shape factor, λ is the X-ray wavelength, β is the line broadening at half the maximum intensity, and θ is the diffraction angle.

3.7 | SEM and EDX spectra

Four SEM micrographs (Figure 8) of $[Cd_2LCl(H_2O)_6]$ were recorded at 300 nm (a), 10 μm (b), 1 μm (c), and 1 μm magnified (d). These micrographs gives the surface morphology of the complex. The SEM images show the rock-shaped structure. The presence of Cd, Cl, S, O, and C in $[Cd_2LCl(H_2O)_6]$ complex was confirmed from the energy dispersive X-ray analysis graph (Figure 9).

3.8 | Thermogravimetric analysis (TGA) and Differential thermal analysis (DTA) studies

The TGA and DTA studies of the samples were carried out at 0–1000°C. The metal complexes displayed a similar type of thermal decomposition. The TGA and DTA studies of the $[Co_2LCl(H_2O)_6]$ complex are discussed here (Figures 10 and 11). The Co(II) complex was stable up to 138°C. However, there was a decrease in the mass of 19.27%, consistent with the loss of six coordinated water molecules shown at 145°C. The anhydrous metal complexes showed rapid degradation after 300°C for the coordinated chlorine atom and organic moiety. The degradation continued up to ~579°C, as indicated in the plateau of the thermogram. Finally, the corresponding stable metal oxide was obtained, constituting 26.78% of the total mass of the complex. The TGA data for all the metal complexes are listed in Supporting Information Table S2. The kinetic parameters such as the order of the reaction (n) and the activation energy (E_a) can be found from Freeman–Carrol equation[47]:

$$-dw/dt = R_T = Z/R_H e^{-Ea/RT} W^n$$

where R_H is the rate of heating, W is the weight fraction of the reacting material, E_a is the activation energy, and Z is the frequency factor.

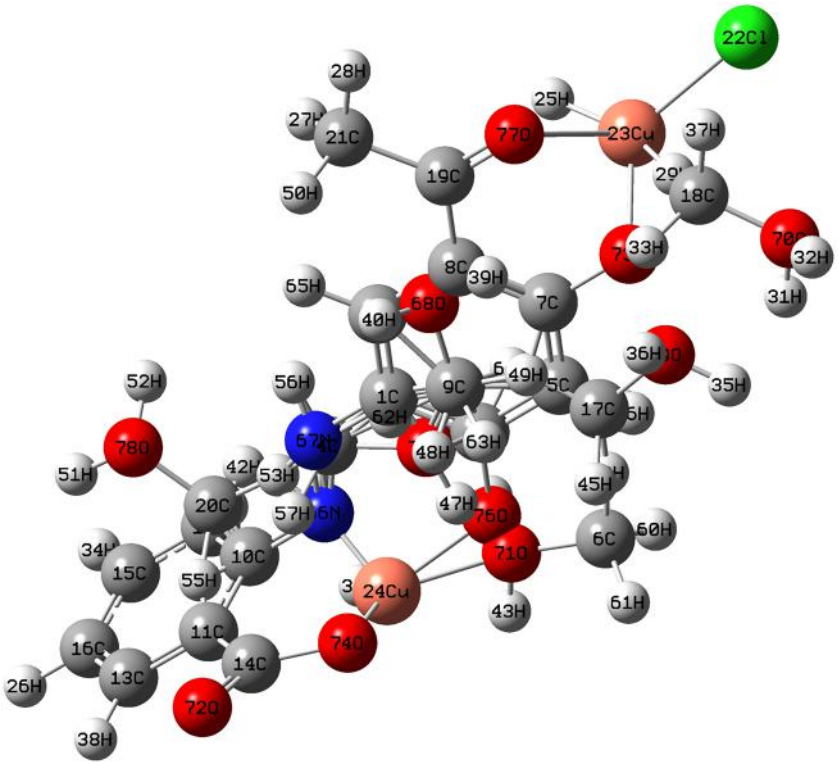

FIGURE 16 Optimized geometry of $[Cu_2(L)Cl(H_2O)_6]$

$$\Delta \log R_T = n\Delta \log W - E_a/2.303R\Delta(1/T)$$

A plot of $\Delta \log R_T$ verses $\Delta \log W$ gives a linear relationship, if $\Delta(1/T)$ is kept constant, where the slope and the intercept provide the values of n and E_a, respectively. Finally, the order of the decomposition reaction (n) and the activation energy (E_a) are found to be 0.4 and 7.37 J/mol, respectively. However, the low calculated value for E_a shows the autocatalytic effect of the metal ions.[48] The correlation factor (r) at 0.87 and the degree of thermal decomposition were in accordance to the experimental findings.

3.9 | Molecular modelling studies

The molecular modelling studies were performed in a GAUSSIAN application platform to ascertain the atomic arrangement around the metal ions. The azo dye ligand and its copper, nickel, manganese, copper, and zinc complexes (Figures 12–17) were optimized using the B3LYP/6–31+G (d, p)/LANL2DZ basis set to set up the geometry theoretically. The bond parameters such as bond lengths and the bond angles of the optimized ligand remarkably recognized with metal complexes (Table 2,3), which explains the mode of bonding of the azo dye ligand to the metal ions.[49,50] The energetic properties of the single point energy and dipole moment (D) of H_3L, $[Co_2(LH_3)Cl(H_2O)_6]$, $[Ni_2(LH_3)Cl(H_2O)_6]$, $[Mn_2(LH_3)Cl(H_2O)_6]$, $[Cu_2(LH_3)Cl(H_2O)_6]$, and $[Zn_2(LH_3)Cl(H_2O)_2]$ were examined by the DFT/B3LYP 6–31+G (d, p) and DFT/B3LYP LANL2DZ basis sets. Furthermore, the single point energy for the ligand was higher in comparison to the complexes, indicating that the complexes are more stable than the azo dye ligand.[26] However, the higher dipole moment for the zinc complex suggests to have maximum dipole–dipole interaction than other complexes.

TABLE 2 Important bond lengths and bond angles of the ligand $(C_{15}H_{12}N_2O_5)H_3L$ to ascertain structure

B3LYP/6.31G (d, p)	
Bond lengths (Å)	**Bond angles (°)**
C8–O31 (1.410)	C11–C8–O31 (119.995)
C9–N29 (1.301)	O31–C8–O34 (120.014)
N28–N29 (1.216)	C1–C2–O33 (120.000)
C2–O33 (1.409)	C7–C2–O33 (120.011)
C6–O32 (1.409)	C7–C6–O32 (119.990)
C15–O30 (1.213)	C5–C6–O32 (120.000)
–	C5–C15–O30 (120.016)
–	C4–C15–O30 (119.989)

3.10 | FMO approach and chemical reactivity measurements studies

The Highest Occupied Molecular Orbital (HOMO) and Lowest Unoccupied Molecular Orbital (LUMO) energies for the azo dye ligand H_3L and its corresponding

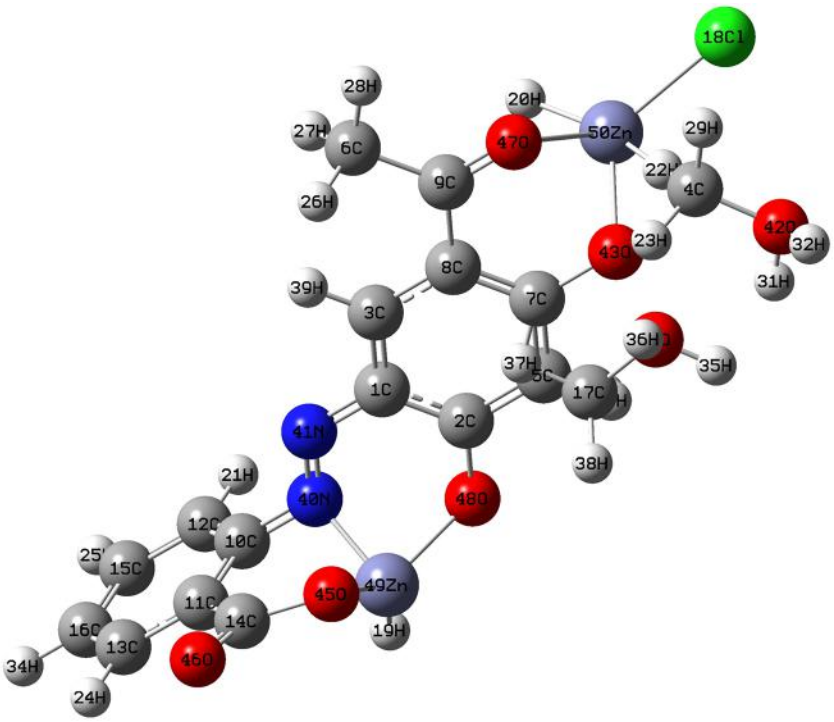

FIGURE 17 Optimized geometry of $[Zn_2(L)Cl(H_2O)_2]$

TABLE 3 Important bond lengths and bond angles of cobalt, nickel, manganese, copper, and zinc complexes to ascertain structure

$[Co_2(LH_3)Cl(H_2O)_6]$ B3LYP/ LANL2DZ		$[Ni_2(LH_3)Cl(H_2O)_6]$ B3LYP/ LANL2DZ		$[Mn_2(LH_3)Cl(H_2O)_6]$ B3LYP/LANL2DZ		$[Cu_2(LH_3)Cl(H_2O)_6]$ B3LYP/LANL2DZ		$[Zn_2(LH_3)Cl(H_2O)_2]$ B3LYP/ LANL2DZ	
Bond length (Å)	**Bond angle (°)**	**Bond length (Å)**	**Bond angle (°)**	**Bond length (Å)**	**Bond angle (°)**	**Bond length (Å)**	**Bond angle (°)**	**Bond length (Å)**	**Bond angle (°)**
O75–Co24 (1.804)	C14–O75–Co24 (96.610)	O76–Ni69 (1.789)	C14–O76–Ni69 (109.923)	O80–Mn68 (1.810)	C14–O80–Mn68 (109.836)	O74–Cu24 (1.816)	C14–O74–Cu24 (100.580)	O45–Zn49 (1.914)	C14–O45–Zn49 (104.031)
C14–O75 (1.409)	N68–N69–Co24 (129.626)	C14–O76 (1.410)	N66–N67–Ni69 (116.751)	C14–O80 (1.410)	N70–N71–Mn68 (116.554)	C14–O74 (1.410)	N67–N66–Cu24 (126.275)	C14–O45 (1.410)	N41–N40–Zn49 (120.703)
N59–Co24 (1.179)	C14–O75–Co24 (96.610)	N67–Ni69 (1.828)	C17–O78–Ni69 (127.156)	N71–Mn68 (1.850)	C2–O74–Mn68 (109.466)	N66–Cu24 (1.850)	C2–O76–Cu24 (109.492)	N40–Zn49 (1.715)	C2–O48–Zn49 (109.448)
N68–N69 (1.217)	N69–Co24–O75 (82.991)	N66–N67 (1.217)	N67–Ni69–O76 (104.072)	N70–N71 (1.216)	N71–Mn68–O74 (79.349)	N66–N67 (1.068)	N66–Cu24–O74 (76.481)	N40–N41 (1.216)	N40–Zn49–O45 (90.554)
O78–Co24 (1.800)	C7–O24–Co23 (109.511)	O78–Ni69 (2.160)	C7–O73–Ni68 (109.500)	O74–Mn68 (1.810)	C7–O78–Mn69 (109.491)	O76–Cu24 (1.810)	C19–O77–Cu23 (107.764)	O48–Zn49 (1.889)	C9–O47–Zn50 (108.382)
O76–Co23 (2.351)	C19–O76–Co23 (107.836)	O77–Ni68 (2.098)	C19–O77–Ni68 (107.794)	O78–Mn69 (1.810)	C19–O81–Mn69 (107.928)	O77–Cu23 (2.352)	C7–O73–Cu23 (109.500)	O47–Zn50 (2.377)	C7–O43–Zn50 (109.505)
O74–Co23 (1.801)	O74–Co23–Cl22 (93.378)	O73–Ni68 (1.955)	O77–Ni68–Cl22 (103.210)	O81–Mn69 (2.353)	O81–Mn69–Cl22 (109.689)	O73–Cu23 (1.809)	O77–Cu23–Cl22 (109.716)	O43–Zn50 (1.890)	O47–Zn50–Cl18 (110.502)
Cl22–Co23 (2.148)	O76–Co23–Cl22 (107.873)	Cl22–Ni68 (2.140)	O73–Ni68–Cl22 (90.010)	Cl22–Mn69 (2.159)	O78–Mn69–Cl22 (119.993)	Cl22–Cu23 (2.160)	O73–Cu23–Cl22 (120.013)	Cl20–Zn50 (2.239)	O43–Zn50–Cl18 (120.029)

complexes were analyzed to calculate the global reactivity descriptors such as chemical potential, electrophilicity, and chemical hardness. The molecular orbital coefficients prominently described that the –N=N– (azo), >C=O (carbonyl), –COO (carboxylic), and C–O (phenolic) groups were the possible binding sites of the ligand H_3L to the metal ions.[51] The negative values of E_{HOMO} and E_{LUMO} confirmed that the ligand and its complexes were stable.[51,52] The electron density for the ligand was localized on O_{31}, O_{30}, O_{32}, O_{33}, and N_{29} in the highest occupied molecular orbitals (Figure 18), suggesting they are suitable for nucleophiles.[53] However, the difference in energy (E_{HOMO} – E_{LUMO}) for the ligand was smaller in comparison to its complexes, except the nickel complex, suggesting the ligand is more reactive and less stable than its complexes (Figure 18).

The charge transfer interaction can be explained on the basis of frontier molecular orbitals and the orbital energy gap. The chemical reactivity values such as electronegativity (χ),chemical potential (μ), global hardness (η), global softness (S), and global electrophilicity index (ω)[54,55] are shown in Table 4.

$$\chi = -\frac{(E_{LUMO} + E_{HOMO})}{2}$$

$$\boldsymbol{\mu = -\chi = \frac{(E_{LUMO} + E_{HOMO})}{2}}$$

$$\boldsymbol{\eta = \frac{(E_{LUMO} - E_{HOMO})}{2}}$$

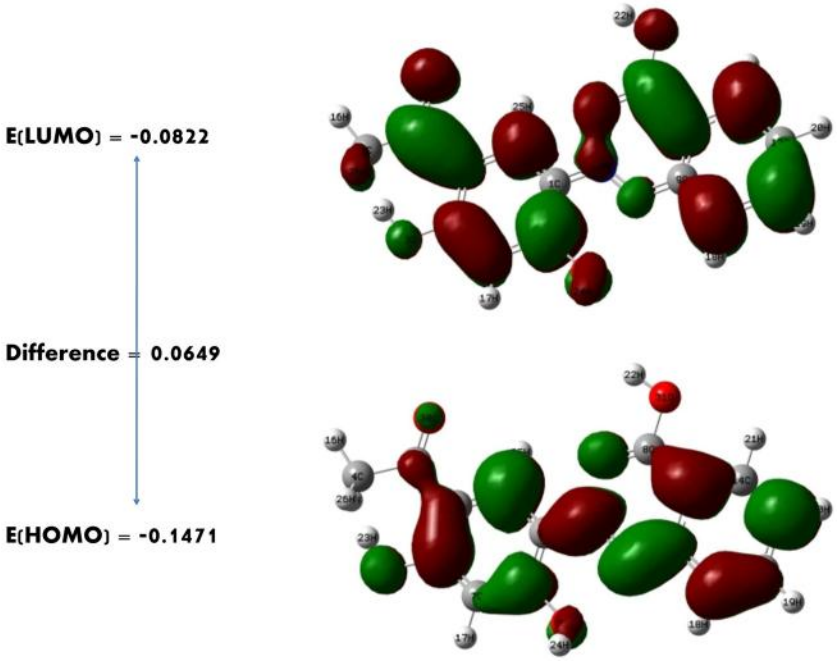

FIGURE 18 Difference between HOMO and LUMO energies of the ligand H_3L

TABLE 4 Energetic properties of the ligand H_3L and its metal complexes calculated by the DFT/B3LYP 6.31+G (d, P) and DFT/B3LYP LANL2DZ basic sets

Compound	Single point energy (kcal/mol)		Dipole moment (*D*)	
	DFT/B3LYP 6.31G+(d, P)	DFT/B3LYP LANL2DZ	DFT/B3LYP 6.31G+ (d, P)	DFT/B3LYP LANL2DZ
$H_3L(C_{15}H_{12}N_2O_5)$	-6.6797×10^6	–	0.376	–
$[Co_2(LH_3)Cl(H_2O)_6]$	-30.1875×10^6	-30.5890×10^6	−1.189	−1.234
$[Ni_2(LH_3)Cl(H_2O)_6]$	-30.8890×10^6	-30.6930×10^6	−1.151	−1.491
$[Mn_2(LH_3)Cl(H_2O)_6]$	-31.5591×10^6	-31.1183×10^6	−1.343	−1.761
$[Cu_2(LH_3)Cl(H_2O)_6]$	-32.2263×10^6	-32.1092×10^6	−1.159	−1.256
$[Zn_2(LH_3)Cl(H_2O)_2]$	-33.3312×10^6	-33.5619×10^6	4.037	3.712

$$S = \frac{1}{2\eta}$$

$$\omega = \frac{\mu^2}{2\eta}$$

$$\sigma = \frac{1}{\eta}$$

The plots for energy comparison between orbitals of the compounds are shown in Figures 19–23. The value for chemical softness (S) for the ligand was smaller in comparison to those for its complexes, suggesting it is more stable. However, the Zn(II) complex was more stable because its electrophilicity (ω) value is lower than that of the other complexes (Table 5).

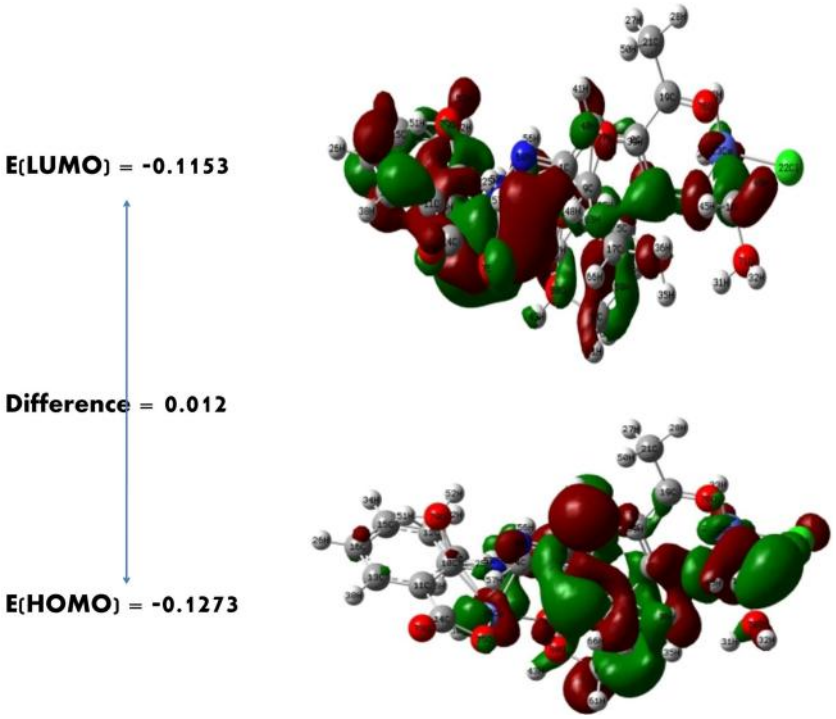

FIGURE 19 Difference between HOMO and LUMO energies of $[Co_2(L)Cl(H_2O)_6]$

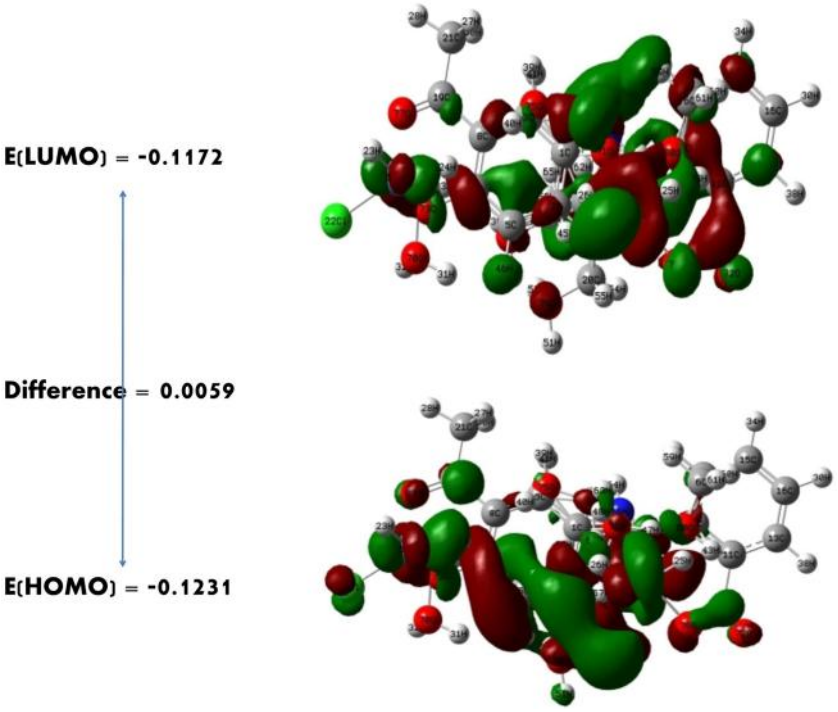

FIGURE 20 Difference between HOMO and LUMO energies of $[Ni_2(L)Cl(H_2O)_6]$

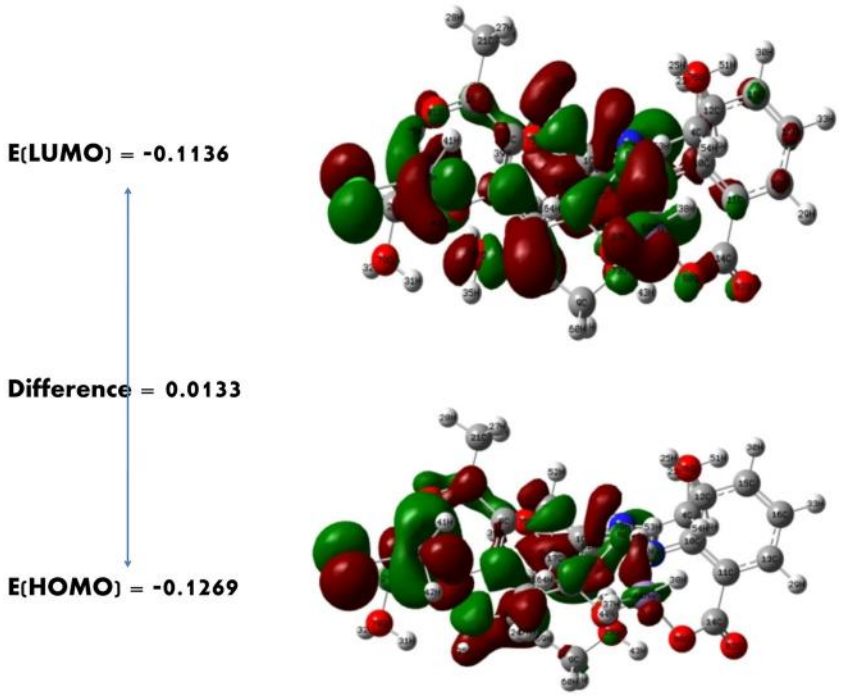

FIGURE 21 Difference between HOMO and LUMO energies of $[Mn_2(L)Cl(H_2O)_6]$

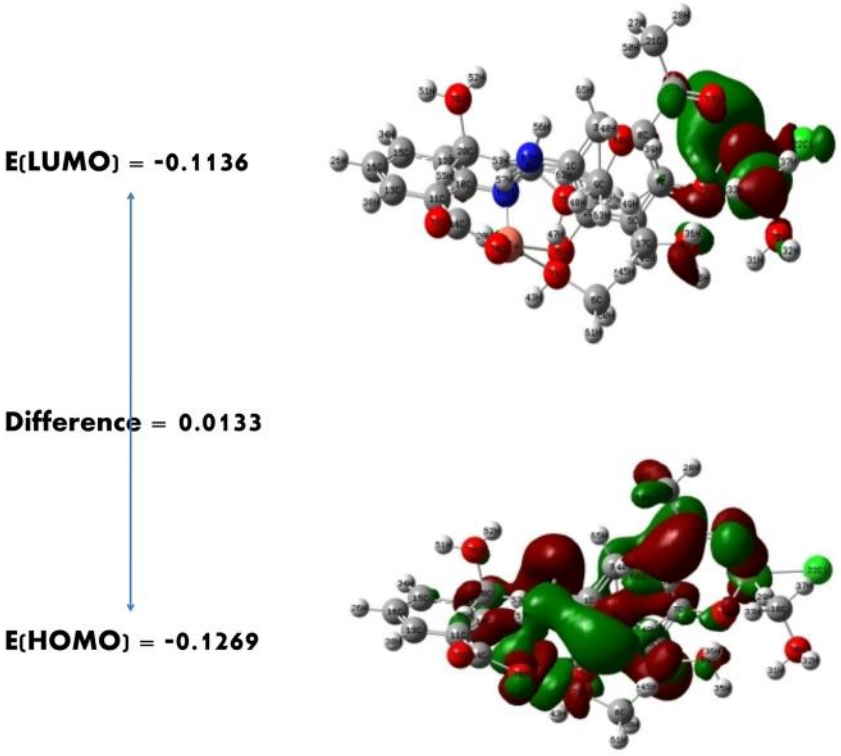

FIGURE 22 Difference between HOMO and LUMO energies of $[Cu_2(L)Cl(H_2O)_6]$

3.11 | Quantitative structure–activity relationship studies

The QSAR method is a useful tool to predict the activity, reactivity, and some common functions of the prepared molecules. All calculations were carried out using the HyperChem Professional 8.0.3 program. The azo dye ligand structure is optimized by using an (MM^+) force field, with semi-empirical PM3 methods. The energy minimization method was fulfilling with the Fletcher–Reeves conjugate gradient algorithm. The calculated partition coefficient (log *P*) value for the azo

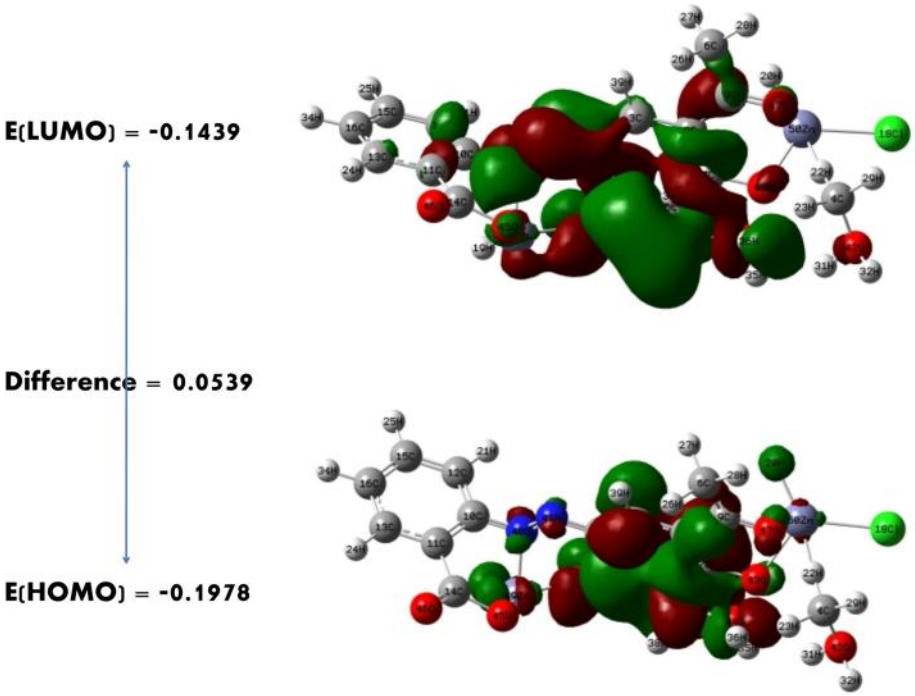

FIGURE 23 Difference between HOMO and LUMO energies of $[Zn_2(L)Cl(H_2O)_2]$

TABLE 5 Calculated quantum chemical parameters for ligands and their metal complexes

Compound	HOMO (eV)	LUMO (eV)	ΔE (eV)	χ (Pauling)	η (eV)	σ	μ (eV)	S	Ω (eV)
$(C_{13}H_{10}N_4O_5)$L1	−0.1471	−0.0822	0.0649	−0.1146	0.0324	30.8641	0.1146	15.4320	0.2021
$[Co_2(LH_3)Cl(H_2O)_6]$	−0.1273	−0.1153	0.012	−0.1213	0.006	166.6666	0.1213	83.3333	1.225
$[Ni_2(LH_3)Cl(H_2O)_6]$	−0.1231	−0.1172	0.0059	−0.1201	0.0029	344.8275	0.1201	172.4137	2.4827
$[Mn_2(LH_3)Cl(H_2O)_6]$	−0.1269	−0.1136	0.0133	−0.1202	0.0066	151.5151	0.1202	75.7575	1.0909
$[Cu_2(LH_3)Cl(H_2O)_6]$	−0.1383	−0.1169	0.0214	−0.1276	0.0107	93.4579	0.1276	46.7289	0.7570
$[Zn_2(LH_3)Cl(H_2O)_2]$	−0.1978	−0.1439	0.0539	−0.1708	0.0269	37.1747	0.1708	18.5873	0.5408

TABLE 6 QSAR Calculation for optimized ligand H_3L

Function	Ligand (2′,4′-dihydroxy-5′-acylphenylazo)-2-carboxybenzene
Surface area (approx.) ($Å^2$)	378.84
Surface area (grid) ($Å^2$)	478.29
Volume ($Å^3$)	791.46
Hydration energy (kcal/mol)	−18.60
Log*P*	6.08
Refractivity ($Å^3$)	21.82
Polarizability ($Å^3$)	29.74
Mass (amu)	300.27
Total energy (kcal/mol)	−86406.5
Dipole moment (Debye)	1.84
Free energy (kcal/mol)	−86406.5
RMS gradient (kcal/Å mol)	47.83

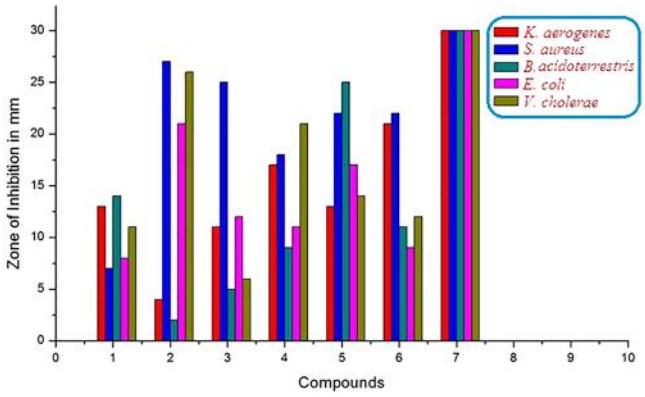

FIGURE 24 Antibacterial activities of the compounds

dye ligand H_3L is 6.08 respectively. The important role of the partition coefficient (log *P*) value is to describe the biological activity of the prepared azo dye ligand and to measure the permeability of the applied prepared ligands into the cell membrane.[55] Other important required physical parameters such as surface area, volume, hydration energy, refractivity, polarizability, mass, total energy, free energy and Root mean square (RMS) gradient were also evaluated to determine the activity of the azodye ligand, and these are listed in Table 6.

3.12 | Antibacterial activity

The compounds were screened against *K. aerogenes*, *S. aureus*, *B. acidoterrestris*, *E. coli*, and *V. cholerae* and the zone of inhibition is shown in Figure 24 (Supporting Information Table S3). The synthesized compounds displayed significant activity against all tested strains. Again the metal complexes show better activity than the free ligand, which may be explained on the basis of overtone concept and chelation theory.[56] Furthermore, the increase in activity may also be due to the effect of a decrease in the polarizability, which could enhance the lipophilicity of the chelates. This leads to a breakdown of the permeability of the cells, resulting in interference with normal cell processes. Tetracycline is used as the standard reference while DMSO is used as the negative control. For all the complexes, the partition coefficient (*C*log*P*) values show good results with an average of 6.438, which explains their better biological activity because *C*log*P* plays a

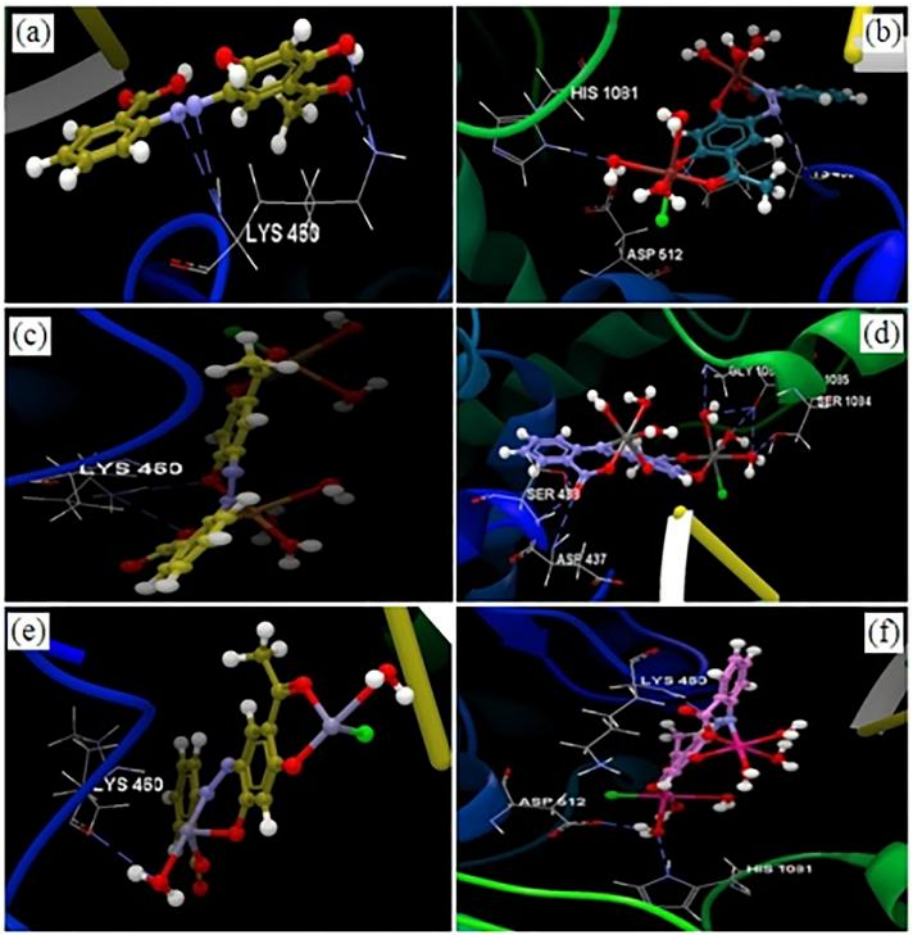

FIGURE 25 (a) Hydrogen bonds between the residues of LYS 460 and (a) H_3L, (b) $[Ni_2LCl(H_2O)_6]$, (c) $[Cu_2LCl(H_2O)_6]$, (d) $[Mn_2LCl(H_2O)_6]$, (e) $[Zn_2LCl(H_2O)_2]$, and (f) $[Co_2LCl(H_2O)_6]$

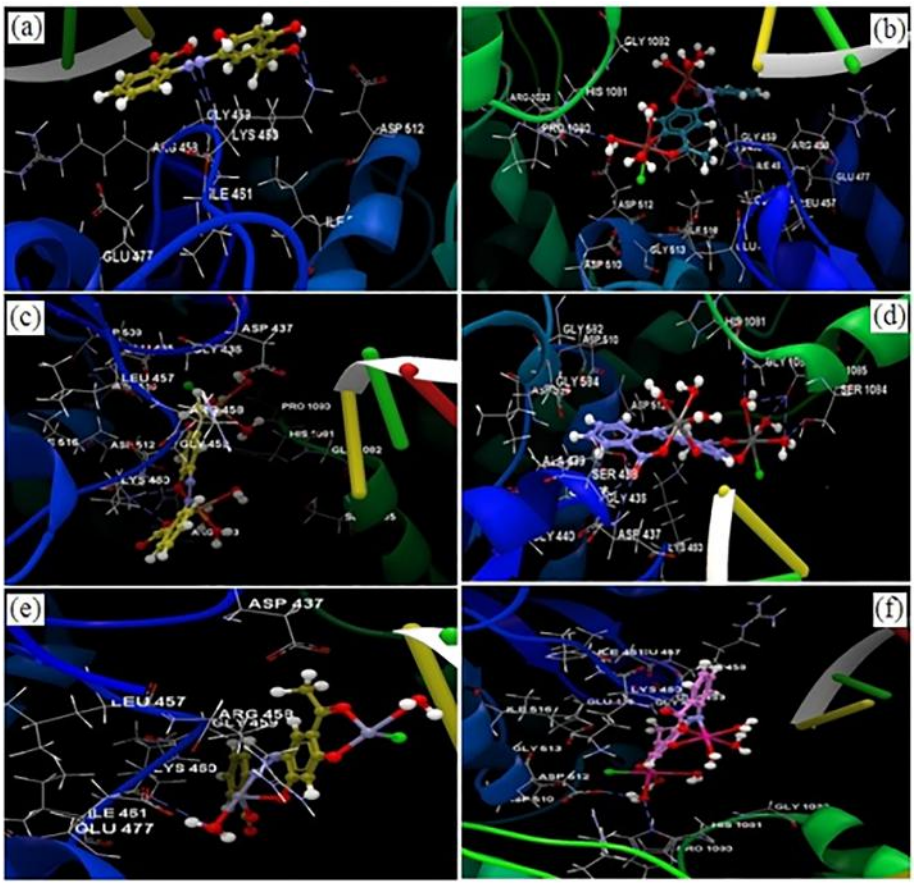

FIGURE 26 (a) Docking pose of (a) H_2L, (b) $[Ni_2LCl(H_2O)_6]$, (c) $[Cu_2LCl(H_2O)_6]$, (d) $[Mn_2LCl(H_2O)_6]$, (e) $[Zn_2LCl(H_2O)_2]$, and (f) $[Co_2LCl(H_2O)_6]$ interacting with amino acid residues

TABLE 7 Calculated properties of compounds

Compound	Atoms	Weight (Daltons)	Flexible bonds	Lipinski violations	Hydrogen donors	Hydrogen acceptors	Log*P*
Cp	41	330.33	3	0	1	6	1.17
H_3L	36	302.28	4	0	3	7	4.07
$[Co_2LCl(H_2O)_6]$	52	558.65	0	3	12	13	1.97
$[Ni_2LCl(H_2O)_6]$	52	558.17	0	3	12	13	1.97
$[Cu_2LCl(H_2O)_6]$	52	567.88	0	3	12	13	1.97
$[Mn_2LCl(H_2O)_6]$	52	550.56	0	3	12	13	1.97
$[Zn_2LCl(H_2O)_2]$	40	499.54	0	0	4	9	3.86

major role in the permeability of the tested compounds into the cell membrane.

3.13 | Docking studies

Molecular docking studies were carried out according to the docking protocol.[57] The validation of the method and docking parameters was performed by redocking the co-crystallized. The docking score and hydrogen bonds created with the amino acids were used to predict the binding modes, binding affinities, and orientation of the docked compounds in the active site of the protein receptor. The molecular properties, such as the parameters of Lipinski's rule of five (molecular weight, number of hydrogen bond acceptors, number of hydrogen bond donors and logP, the octanol–water partition coefficient) were computed using Calculate Molecular Properties tool.[58] The protein–ligand complex was realized based on the crystal structure of *S. Aureus* DNA GYRASE (PDB ID: 2XCT) downloaded from the Protein Data Bank.[59]

The docking pose, binding site, and binding pocket of the co-crystallized ciprofloxacin (Cp) interacting with amino acid residues are shown in Supporting Information Figure S1. To ensure that the ligand orientations and position obtained from the molecular docking studies are valid, the docking methods and parameters used were validated by redocking. The docking score and hydrogen bonds formed with the amino acids are listed in Supporting Information Table S4 and shown in Figures 25 and 26. The co-crystallized Cp (score −34.59, RMSD 0.05) forms one hydrogen bond, with LYS 460 (bond length 2.885 Å). After performing the molecular docking study, it was observed that most of the compounds had the same orientation as the co-crystallized Cp, as shown in Supporting Information Table S4. Only $[Mn_2LCl(H_2O)_6]$ adopted a different orientation to that of the co-crystallized. The $[Mn_2LCl(H_2O)_6]$ (docking score −31.46, RMSD 0.02) showed there were eight hydrogen bonds with SER 438 (3.060 and 2.782 Å), ASP 437 (2.879 Å), R 1084 (2.776 Å), SER 1085 (2.727, 2.984 and 2.996 Å), and GLY 1082 (3.192 Å).

According to the docking score evaluation, it was observed that $[Ni_2LCl(H_2O)_6]$ had a significant docking score (−35.30, RMSD: 0.01) (better than co-crystallized Cp) and formed three hydrogen bonds with LYS 460 (bond length 3.123 Å), ASP 512 (bond length 3.068 Å), and HIS 1081 (bond length 3.118 Å). The compound $[Cu_2LCl(H_2O)_6]$ also had a better docking score (−33.13, RMSD 0.02 Å) and had two hydrogen bonds with LYS 460 (2.767 and 2.940 Å). The ligand H_3L had four hydrogen bonds with LYS 460 (3.200, 3.162, 3.116, and 3.059 Å) (Figure 25). All the metal complexes had better docking scores than the azo dye ligand (−31.08, RMSD 0.69). The docking poses of all the compounds in the ligand binding site of 2XCT are shown in Supporting Information Figure S2. The calculated parameters (Table 7) can predict whether a molecule has properties that might turn it into an active drug according to Lipinski's rule of five[58]: number of hydrogen donors <5, number of hydrogen acceptors <10, molecular weight <500 Da, octanol–water partition coefficient (log*P*) <5.

4 | CONCLUSION

A novel pentadentate azo dye ligand H_3L and its series of binuclear metal complexes was successfully synthesized and structurally investigated. Thermal and morphological analysis for these compounds was also performed. The kinetic parameters, such as order and activation energy, were determined from the thermal decomposition values. Powder XRD analysis revealed the orthorhombic nature of the cadmium complex. The compounds were also optimized using the Gaussian 03 program and all the calculations were done theoretically, which explains the mode of bonding. Furthermore, the synthesized compounds displayed potent antibacterial activity against all tested strains. The metal complexes showed better activity than the free ligand, which may be explained on the basis of chelation theory. Moreover, molecular docking analysis was carried out and the interactions occurring in the protein–ligand complexes were predicted. This study will undeniably help researchers in designing new drugs using this class of compounds.

ACKNOWLEDGMENTS

The authors are also thankful to I.I.P Dehradun, India for providing spectral analysis, SEM, EDX, XRD, and thermo gravimetric analysis. The first and corresponding author (Dr. Ashish K. Sarangi) is highly thankful l to (Mrs Suprava Dash) for her valuable time and support in preparing the manuscript.

ORCID

Ashish Kumar Sarangi https://orcid.org/0000-0002-5602-4736
Bipin Bihari Mahapatra https://orcid.org/0000-0002-3758-6821
Ranjan Kumar Mohapatra https://orcid.org/0000-0001-7623-3343
Lucia Pintilie https://orcid.org/0000-0002-1036-7653
Mohammad Azam https://orcid.org/0000-0002-4274-2796

REFERENCES

[1] H. A. Sahyon, A. A. El-Bindary, A. F. Shoair, A. A. Abdellatif, *J. Mol. Liq.* **2018**, *255*, 122.
[2] M. M. El-ajaily, A. K. Sarangi, R. K. Mohapatra, S. S. Hassan, R. N. El-daghare, P. K. Mohapatra, M. K. Raval, D. Das, A. Mahal, A. Cipurkovic, T. H. Al-Noor, *ChemistrySelect* **2019**, *4*, 9999.
[3] S. M. Soliman, J. H. Albering, E. N. Sholkamy, A. El-Faham, *Appl. Organometal. Chem.* **2020**, e5603. https://doi.org/10.1002/aoc.5603
[4] R. K. Mohapatra, P. K. Das, M. M. El-ajaily, U. Mishra, D. C. Dash, *Bull. Chem. Soc. Ethiop.* **2018**, *32*(3), 437.
[5] R. K. Mohapatra, A. K. Sarangi, M. Azam, M. M. El-ajaily, M. K. Zahan, S. B. Patjoshi, D. C. Dash, *J. Mol. Struct.* **2019**, *1179*, 65.
[6] H. Xu, X. Zeng, *Bioorg. Med. Chem. Lett.* **2010**, *20*, 4193.
[7] M. Gaber, S. K. Fathalla, H. A. El-Ghamry, *Appl. Organometal. Chem.* **2019**, e4707. https://doi.org/10.1002/aoc.4707
[8] F. A. Saad, H. A. El-Ghamry, M. A. Kassem, *Appl. Organometal. Chem.* **2019**, e4965. https://doi.org/10.1002/aoc.4965
[9] W. H. Mahmoud, F. N. Sayed, G. G. Mohamed, *Appl. Organometal. Chem.* **2018**, e4347. https://doi.org/10.1002/aoc.4347

[10] S. A. Abouel-Enein, S. M. Emam, E. Monir, *Appl. Organometal. Chem.* **2018**, e4191. https://doi.org/10.1002/aoc.4191
[11] I. M. El-Deen, A. F. Shoair, M. A. El-Bindary, *J. Mol. Struct.* **2019**, *1180*, 420.
[12] F. Karipcin, B. Dede, S. Percin-Ozkorucuklu, E. Kabalcil, *Dyes Pigm.* **2009**, *84*, 14.
[13] B. B. Mahapatra, R. R. Mishra, A. K. Sarangi, *Bull. Chem. Soc. Ethiop.* **2016**, *30*(1), 87.
[14] B. B. Mahapatra, R. R. Mishra, A. K. Sarangi, J. Saudi, *Chem. Soc.* **2016**, *20*, 635.
[15] B. B. Mahapatra, R. R. Mishra, A. K. Sarangi, *J. Chem.* **2013**, 1. https://doi.org/10.1155/2013/653540
[16] B. B. Mahapatra, S. N. Chaulia, A. K. Sarangi, S. N. Dehury, J. R. Panda, *J. Mol. Struct.* **2015**, *1087*, 11.
[17] GaussView 5.0, (Gaussian Inc., Wallingford, CT, USA) **2009**.
[18] A. D. Becke, *J. Chem. Phys.* **1993**, *98*(7), 5648.
[19] C. T. Lee, W. T. Yang, R. G. Parr, *Phys. Rev. B* **1988**, *37*, 785.
[20] A. D. Becke, *Phys. Rev. A* **1988**, *88*, 1053.
[21] P. J. Hay, W. R. Wadt, *J. Chem. Phys.* **1984**, *82*(1), 270.
[22] P. J. Hay, W. R. Wadt, *J. Chem. Phys.* **1985**, *82*, 284.
[23] P. J. Hay, W. R. Wadt, *J. Chem. Phys.* **1985**, *82*, 299.
[24] M. J. Frisch, G. W. Trucks, H. B. Schlegel, G. E. Scuseria, D. J. Fox, T. Keith, M. A. Al-Laham, C. Y. Peng, A. Nanayakkara, M. Challacombe, P. M. W. Gill, B. Johnson, W. Chen, M. W. Wong, C. Gonzalez, and J. A. Pople, Gaussian, Inc., Wallingford CT GAUSIAN 03, Revision E.01, Gaussian Inc.: Pittsburgh, PA, **2004**.
[25] M. J. Pelczar, J. D. Reid, *Microbiology*, Tata Mcgraw Hill, New Delhi **1974** 473.
[26] A. K. Sarangi, B. B. Mahapatra, S. K. Sethy, *Chem. Afr.* **2018**, *1*, 17.
[27] L. K. Mishra, B. N. Keshari, *Indian J. Chem. Sect-A.* **1981**, *28*, 883.
[28] R. B. King, M. B. Bisnette, *Inorg. Chem.* **1966**, *5*, 300.
[29] K. Nakamoto, *Infrared and Raman spectra of inorganic and coordination compounds*, John Wiley, NY, USA **1978** 239.
[30] J. R. Ferraro, *Low Frequency Vibration of Inorganic and Coordination compound*, Plenum Press, New York **1971** 321.
[31] P. J. Atkins, D. F. Shriver, *Inorganic Chemistry*, 3rd ed., W.H. Freeman and CO, New York **1999**.
[32] A. B. P. Lever, *Inorganic Electronic Spectroscopy*, Elsevier, Amsterdam, UK **1984** 554.
[33] R. Magee, L. Gordan, *Talanta* **1963**, *10*, 967.
[34] S. Yamada, *Coord. Chem. Rev.* **1966**, *1*, 415.
[35] I. M. Procter, B. J. Hathaway, P. Nicholls, *J. Chem. Soc. a* **1968**, 1678.
[36] A. Tavman, D. Gürbüz, A. Çinarli, S. B. Tan, *Bull. Chem. Soc. Ethiop.* **2015**, *29*(1), 63.
[37] D. H. Williams, I. Fleming, *Spectroscopic Methods in Organic Chemistry*, 4th ed. Vol. 1, Tata Mc Graw Hill **1994**.
[38] W. Jacob, R. Mukherjee, *Inorg. Chim. Acta* **2006**, *359*, 4565.
[39] U. N. Dash, *First Ed. Sultan Chand & Sons* **1995**, *143*.
[40] R. D. Salman, R. D. Farrant, J. C. Lindon, *Spectrosc. Lett.* **1991**, *24*(9), 1071.
[41] A. M. A. Alaghar, *J. Mol. Struct.* **2014**, *1072*, 103.
[42] B. J. Hathway, D. E. Billing, *Coord. Chem. Rev.* **1970**, *5*, 143.
[43] F. K. Kneubuhl, *J. Chemical Physics* **1960**, *33*, 1074.
[44] J. W. Visser, *J. Appl. Crystal* **1969**, *2*, 89.
[45] P. M. de Woulff, *J. Appl. Crystal.* **1968**, *1*, 108.
[46] A. Patterson, *Phys. Rev.* **1939**, *56*(10), 978.
[47] E. S. Freeman, B. Carroll, *J. Phys. Chem* **1958**, *62*(4), 394.
[48] A. Iimura, Y. Inoue, I. Yasumori, *Bull. Chem. Soc. Jpn.* **1983**, *56*, 2203.
[49] T. A. Yousef, T. H. Rakha, U. El-Ayaan, G. M. Abu El-Reash, *J. Mol. Struct.* **2012**, *1007*, 146.
[50] T. A. Yousef, G. M. Abu El-Reash, T. H. Rakha, U. El-Ayaan, *Spectrochim. Acta* **2011**, *83*(1), 271.
[51] T. A. Yousef, G. M. Abu El-Reash, R. M. El Morshedy, *Polyhedron* **2012**, *45*, 71.
[52] T. A. Yousef, G. M. Abu El-Reash, R. M. El Morshedy, *J. Mol. Struct.* **2013**, *1045*, 145.
[53] M. Govindarajan, S. Periandy, K. Carthigayen, *Spectrochim. Acta Part A: Mol. Biomol. Spectrosc.* **2012**, *97*, 411.
[54] R. G. Pearson, *J. Org. Chem.* **1989**, *54*, 1423.
[55] J. Padmanabhan, R. Parthasarathi, V. Subramanian, P. Chattaraj, *J. Phys. Chem.* **2007**, *111*.
[56] K. Mohanan, S. N. Devi, *Russ. J. Coord.* **2006**, *32*, 600.
[57] CLC Drug Discovery Workbench, available from http://www.clcbio.com.
[58] C. A. Lipinski, F. Lombardo, B. W. Dominy, P. J. Feeney, *Adv. Drug Delivery Rev.* **2001**, *46*, 3.
[59] D. B. Bax, P. F. Chan, D. S. Eggleston, A. Fosberry, D. R. Gentry, F. Gorrec, I. Giordano, M. Hann, A. Hennessy, M. Hibbs, J. Huang, E. Jones, J. Jones, K. K. Brown, C. J. Lewis, E. W. May, M. R. Saunders, O. Singh, C. S. Spitzfaden, C. Shen, A. Shillings, A. T. Theobald, A. Wohlkonig, N. D. Pearson, M. N. Gwynn, *Nature* **2010**, *466*, 935.

SUPPORTING INFORMATION

Additional supporting information may be found online in the Supporting Information section at the end of this article.

How to cite this article: Sarangi AK, Mahapatra BB, Mohapatra RK, et al. Synthesis and characterization of some binuclear metal complexes with a pentadentate azodye ligand: An experimental and theoretical study. *Appl Organomet Chem*. 2020;e5693. https://doi.org/10.1002/aoc.5693